ELSEVIER

European Journal of Cancer 41 (2005) 159–167

European Journal of Cancer

www.ejconline.com

Vessel maturation effects on tumour growth: validation of a computer model in implanted human ovarian carcinoma spheroids

L. Arakelyan, Y. Merbl, Z. Agur *

Institute for Medical BioMathematics (IMBM), 10 Ha'Teena St., P.O. Box 282, Bene Ataroth, 60991, Israel
Optimata Ltd., 11 Tuval St., Ramat Gan 52522, Israel

Received 20 April 2004; received in revised form 5 August 2004; accepted 7 September 2004
Available online 18 October 2004

Abstract

We analysed measurements of tumour growth, neovascular maturation and function in human epithelial ovarian carcinoma xenografts, studied noninvasively by magnetic resonance imaging. Results suggest that vascular maturation and mature and immature vessel regression occur continuously during tumour neovascularisation. Moreover, in these spheroids, a high tumour growth-rate is associated with monotonic changes in vessel density (VD) and with large proportions of mature blood vessels, whereas a lower tumour growth-rate is associated with fluctuating VD and lower proportions of mature vessels. These results corroborate a mathematical model for tumour dynamics, including vascular maturation and immature and mature vessel regression. The model predicts that rapid tumour growth may result from a high maturation-rate of neo-vasculatures, due to substantial mature VD in the microenvironment, while a slower tumour growth is an outcome of a lower background VD, leading to a lower vessel maturation-rate, larger proportion of immature vessels and, consequently, to regression-driven instabilities. The generality of these results for other tumour types should be validated.

Keywords: Angiogenesis; Microenvironment; Vascular maturation; Regression; Spheroid; Mathematical model

1. Introduction

Tumour growth and vascularisation is a complex multi-step process involving many interacting stimulatory and inhibitory forces, operating on several levels of biological organisation, on several time-scales and in different rates [1–5]. The versatile balance between these forces, and, most notably, between vessel density (VD) and parenchyma cell numbers within the tumour determines the net tumour growth-rate.

As the complex dynamics of tumour vascularisation are too intricate to be fully understood by intuition alone, it seems essential to develop a formal computerised model for calculating these dynamics under different conditions and different parameter ranges. This challenge consists of three major steps: (i) a mathematical model is constructed, theoretically analysed and computer implemented; (ii) the parameters of the computerised model are adjusted to fit specific tumour types, the adjusted model is simulated for generating predictions about tumour and vasculature dynamics, and the ability of experiments, using the same tumour types, to corroborate the model predictions is examined; (iii) the model is employed for predicting disease progression under different therapeutic regimens.

Recently, the complex interactive hierarchical processes involved in angiogenesis have been analysed in a mathematical model, which takes into account vessel

* Corresponding author. Tel.: +972 3 9733075; fax: +972 3 9733410.
E-mail address: agur@imbm.org (Z. Agur).

0959-8049/$ - see front matter © 2004 Elsevier Ltd. All rights reserved.
doi:10.1016/j.ejca.2004.09.012

maturation and the destabilisation of mature vessels as inherent constituents of tumour growth and angiogenic dynamics [6–9]. The model operates both on the tissue level, i.e., tumour volume and vascular density, on the cellular level, i.e., endothelial cells [10], as well as pericytes [11,12], and on the molecular level, i.e., concentration of growth factors – vascular endothelial growth factor (VEGF) [13–18] and angiopoietins [19].

The simulations of the model suggest that a specific set of ovary carcinoma parameters, yields monotonic growth of both blood vessels and tissue. In this state, all the forces driving the system operate in concert, tumour neovascularisation is well balanced by vessel maturation, and the net tumour growth-rate is maximal. Perturbation of this tumour-vessel growth balance occurs if at least one parameter in the system is off-set. The result is a transition into a fluctuating regime of both neovascularisation and vascular maturation, leading to less efficient perfusion and to a smaller net tumour growth-rate [6,7].

The work presented here was aimed at validating the above mathematical model by comparing its predictions to dynamic measurements of tumour growth and vascularisation dynamics. In particular, we verified the model's assumptions that immature vessel regression and mature vessel destabilisation are significant constituents of *in vivo* tumour vasculature dynamics and that, in different tumours, vessel maturation may vary in rate, thus affecting the overall tumour growth pattern.

2. Materials and methods

2.1. In vivo experiments

For validating the mathematical model, which relates angiogenesis and vessel maturation to the rate of tumour growth, it was essential to monitor individual tumour dynamics, in conjunction with neovasculature formation and maturation. To this end, we employed data from laboratory experiments in which MLS human epithelia ovarian carcinoma spheroids were grafted subcutaneously (s.c.) in the lower back of 13 female CD1-nude mice. Tumour volume, V_T, was monitored for each individual tumour, T, by 5–25 magnetic resonance imaging (MRI) measurements for each tumour. Individual tumour growth curves were obtained by determining the tumour volume non-invasively from two orthogonal high-resolution gradient echo MR images (a detailed description of the experiment is published in [21]).

Three types of vascular signals were monitored for each tumour at each time-point:

1. **Apparent** VD (AVD); this was done by acquiring averaged signal intensity maps during inhalation of air and carbogen and air and air–CO_2 (see Gilead and colleagues [21] for further details); note that the experimental estimation units rely on the measurement instrument, i.e., MRI, rather than on biological dimensions. In order to normalise these data, we calculated the ratio between the signal intensity in a ring of 1 mm surrounding the implanted spheroid (Rim), and the signal intensity in a control region (d) as follows: $\mathrm{AVD} = 1 - \ln S_{\mathrm{Rim}}/S_{\mathrm{d}}$, where S is the signal intensity [20–23] normalised around 1 by the $1-\ln$ term in order to rule out negative values. Note that "AVD" is an experimental parameter, not to be confused with the model units of **average** vessel density, which reflect the ratio between vessel number and tumour volume. These VD units are similar, but not identical.

2. **Mature** VD (MatVD), was estimated by monitoring signal changes in response to hypercapnia; 3. **Functional**, perfused, VD (FunVD), was estimated by monitoring signal changes in response to hyperoxia. These signals were monitored simultaneously in four different sites: the tumour centre (In), an arbitrary point located within the 1 mm wide rim around the tumour spheroid (Rim), and two control points: at a distance of 7 mm from the tumour (c), and a further reference point at a greater distance from the tumour spheroid, in the same tissue (d). Signal intensities, FunVD and MatVD, were calculated by dividing each signal by the corresponding signal in the control regions (in site c or d).

As vasoreactivity and function are measured by different MRI procedures, their comparative assessment requires previous calibration. In order to calibrate MRI signals for FunVD with those of MatVD, we assumed a calibration coefficient K_{Control}, measuring the ratio between readings of FunVD and MatVD in the normal subcutaneous tissue, as well as in the tumour (K_{In}, K_{Out}). In the normal tissue, all vessels are mature. Therefore, K_{Control} should be equal to unity. In contrast, in the tumour, a value of $K_{\mathrm{Control}} \neq 1$ reflects the difference between the two signal intensity measurement techniques.

Thus, using the control area as a reference point, we calibrated the densities of the different vessels inside and outside the tumour as follows: First, we calculated the ratio between MRI signal measurements inside the tumour

$$K_{\mathrm{Control},} = \left(\frac{(\mathrm{FunVD}_{\mathrm{Control}})}{(\mathrm{MatVD}_{\mathrm{Control}})}\right),$$

$$K_{\mathrm{In}} = \left(\frac{(\mathrm{MatVD}_{\mathrm{In}})}{(\mathrm{FunVD}_{\mathrm{In}})}\right) * K_{\mathrm{Control}}.$$

Based on the above calculations, we computed the proportion of mature vessels in the vasculature in each region of the tumour. For example, the calibrated proportion of MatVD inside the tumour, $\mathrm{MatVD_{In}}$, is calculated as follows:

$$\mathrm{MatVD_{In}} = \left(\frac{(\mathrm{FunVD_{Control}})^2 * (\mathrm{MatVD_{In}})}{(\mathrm{MatVD_{Control}})^2 * (\mathrm{FunVD_{In}})}\right) \times \mathrm{FunVD_{In/Control}}.$$

The calibrated proportions were multiplied by FunVD (the functional VD – including both mature and immature vessels) in the same regions in order to retrieve an estimate of MatVD (a alue rather than percentage).

2.2. Tumour growth

The MRI measurements of tumour volume over time $V_{T,t(x)}$ (where individual tumours were indexed alphabetically and $t(x)$ stands for the measurement day) were employed for calculating the daily individual tumour volume growth-rate, r_T, as follows:

$$r_{T(x)} = \left(\frac{V_{T,t(x)}}{V_{T,t(x-1)}}\right)^{\frac{1}{(t(x)-t(x-1))}}.$$

This equation relies on results suggesting a Power Law tumour growth function [24].

2.3. Model structure

The mathematical model is fully described elsewhere [6]. It consists of several sub-compartments of solid tumour growth and vascularisation (Fig. 1), namely, tumour growth module (e.g., proliferation and apoptosis of tumour cells), angiogenesis module (e.g., endothelial cell counts and VEGF concentration) and maturation module (e.g., pericyte counts, platelet-derived growth factor (PDGF), and angiopoietin concentrations). Each module calculates many different variables, and the modules interact with one another to predict dynamic changes in all of the calculated quantities. Each simulation produces a set of graphs representing the changes over time of the different variables. In this work, we describe the vessel density and tumour growth analysis for the validation of the model.

2.4. Parameter evaluation

In order to predict tumour growth and VD dynamics of individual ovary carcinoma spheroids, it was required to implement in the model specific parameters of the biological system at hand, within their known parameter range. These include the various reaction rates of tumour cells, endothelial cells, pericytes and different growth factors interactions, e.g., VEGF mRNA half-life (mean 1.1 h, range 0.89–2.3 h). As most of these parameters are not measurable by current experimental

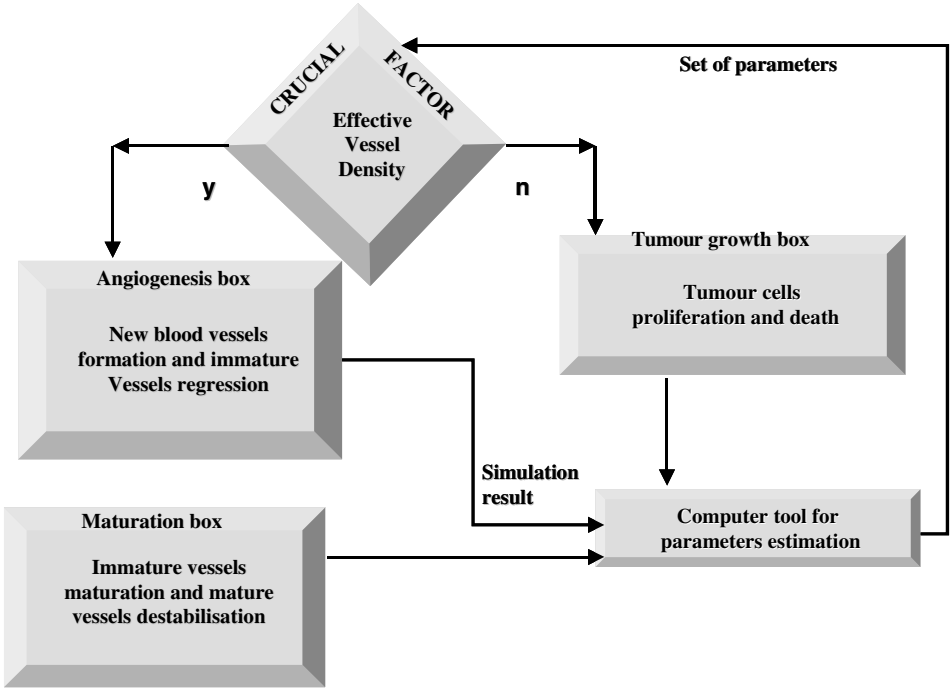

Fig. 1. A general description of the mathematical model of solid tumour dynamics. The model consists of several sub-compartments of solid tumour growth and vascularisation, namely, tumour growth module, angiogenesis module and maturation module. Each module calculates many different variables, and the modules interact with one another to predict dynamic changes in all of the calculated quantities. y, yes; n, no.

methods, we evaluated 87 parameters, consisting of the relevant biological parameters as well as those relating to the mathematical model, by iterative adjustment of the model parameters. The adjustment employed the mathematical model for vascular tumour dynamics [6], a partial set of temporal spheroid volume readings from the present experiments and an efficient search algorithm (modified Powell's conjugate directions method). The set of parameters, which best retrieved the empirical average tumour volume changes over time, was defined as representing the average spheroid in this experiment. This set of parameters was implemented in the model, now representing the average spheroid, for retrieving an independent group of spheroid growth results from the same experiment. It should be noted that in our simulations, background VD at tumour growth initiation was determined arbitrarily, since this parameter could be evaluated by the *in vivo* experiment only a few days following tumour implantation.

3. Results

3.1. Model predictions

Assuming that the implanted spheroids varied mainly in the initial proportion of mature vessels in their implantation sites, we simulated growth and vascularisa-

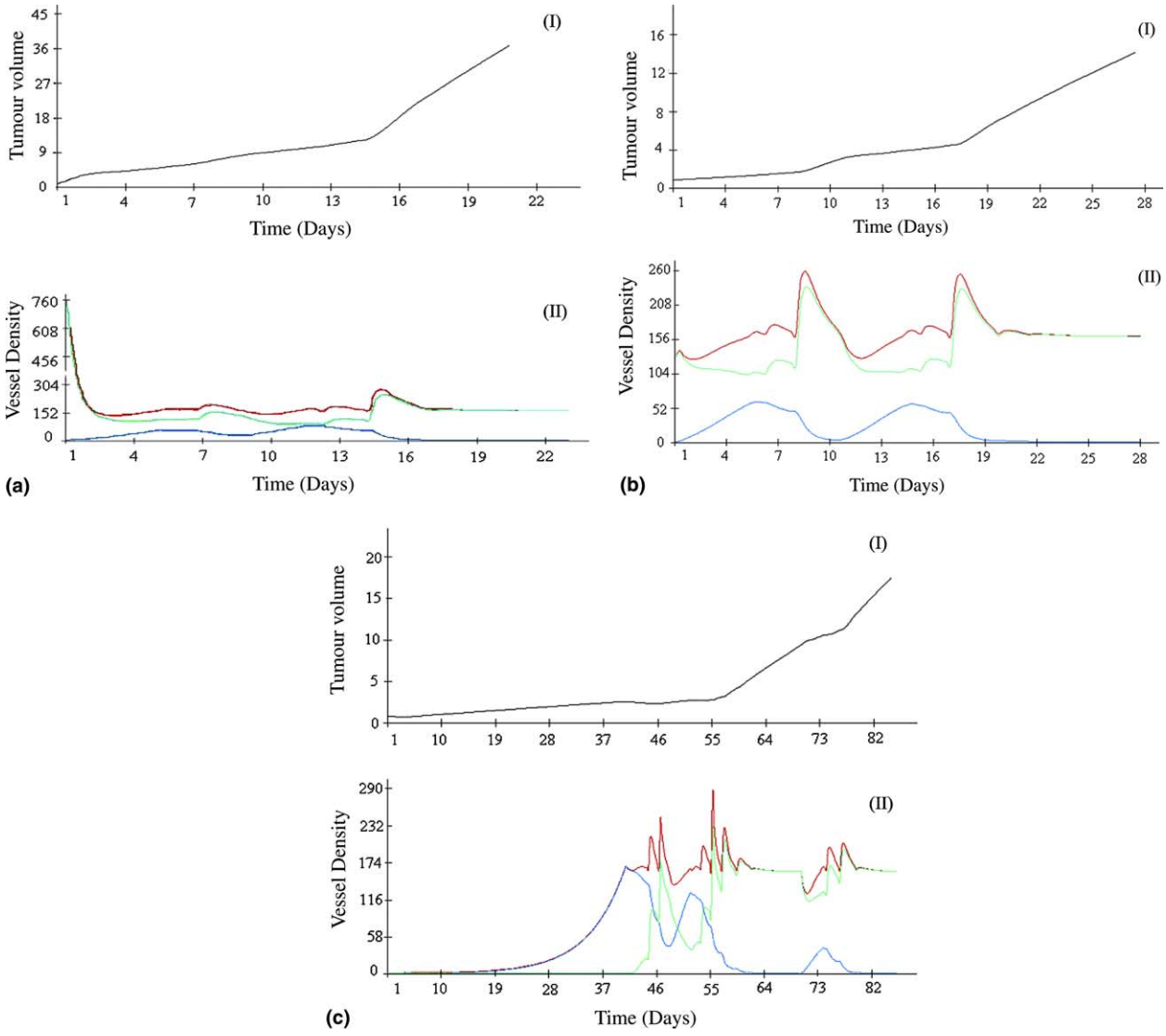

Fig. 2. Simulations of the vascular tumour growth model showing relatively fast (2a), moderate (2b) and slow (2c) growing tumours. Tumour volume (mm^3; I) and vessel density (VD) (μm^3; II) as calculated by the model, using the estimated average spheroid parameters, varying only in initial VD, were plotted as a function of time (days). The total VD, mature vessel density (MatVD), and immature vessel density (ImmVD) are denoted by red (top curve), green (middle curve) and blue (bottom curve), respectively. Note the difference in dimensions between the biological range of VD, as calculated by the model in this figure, and the VD dimensions appearing in Figs. 4 and 5, which reflect magnetic resonance imaging (MRI) procedures.

tion in different tumours in the experiment, using the 87 parameters that were evaluated (data not shown; see Section 2), and evaluating for each tumour the initial density of the mature vessels in the implanted tumour microenvironment. The simulation results were classified according to the predicted rate of each tumour growth.

Three typical examples of the simulation results are shown in Fig. 1(a)–(c), displaying temporal changes in tumour volume, total VD, Immature VD (ImmVD) and MatVD. Thus, when background MatVD was assumed to be relatively high, i.e., 818VD units (each unit equals approximately 55 000 μm^3 mature VD), the tumour increased in size to 45 mm^3 in 1 month and the VD profile exhibited two maximal points (Fig. 2(a)). When background MatVD was taken as 138VD units, the tumour achieved only approximately one third of the previous growth (15 mm^3) in 1 month, and the VD profile had two high peaks intersected by a series of smaller oscillations (Fig. 2(b)). By contrast, simulations of a tumour whose background MatVD was taken as 0.2 VD units (Fig. 2(c)), showed tumour growth of only 2 mm^3 in 1 month and a VD profile which fluctuated with a relatively high frequency and amplitude. Based on these simulations, it is predicted that when the tumour vascular bed is relatively dense, the vessel maturation-rate is high, so that already in the first weeks of spheroid growth most of the vessels are mature. As a result, perfusion is efficient and the tumour grows relatively fast (Fig. 2(a)(II)). This is not the case for slow-growing tumours where the decreased background VD and, hence, decreased vessel maturation-rate bring about a significant regression of immature vessels. This was also discussed in the paper of Gilead and colleagues [21] where only the group of dormant tumours were analysed. Fluctuations in ImmVD can be out of phase with the fluctuations in MatVD and, consequently, the two fluctuating processes show distinguishable episodes of angiogenesis and regression, often alternating with episodes of maturation and destabilisation of mature vessels (Fig. 2(c)(II)).

Interestingly, although the simulated mathematical model assumes that all of the reaction rates are constant and the processes are continuous, the resulting tumour growth can exhibit a dormancy-like period, followed by a faster growth.

3.2. Model validation

3.2.1. Variability in empirical tumour growth-rates

Experimental results (Fig. 3) show that the initially similar tumour spheroids, implanted in genetically similar mice, varied widely in their growth-rates: some of them grew almost exponentially, exceeding 60 mm^3 in only 20 days. The volume increase of moderately growing spheroids was characterised by occasional mild perturbations in the otherwise smooth "Power Law"-like growth curve [25]. In contrast, slow-growing spheroids demonstrated several abrupt changes in the rate of increase. These tumours reached less than 20 mm^3 in 87 days. Taken together, tumour volumes at the end of the laboratory experiment ranged between 14 and 75 mm^3.

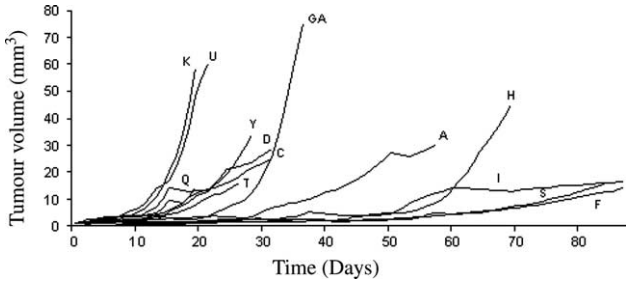

Fig. 3. Experimental results showing *in vivo* tumour growth dynamics as detected noninvasively by blood oxygenation-level-dependent contrast magnetic resonance imaging (MRI). Each MLS human epithelia ovarian carcinoma spheroid was sub-cutaneously (s.c.) implanted in a different female CD1-nude mouse and the tumour volume was monitored as a function of time. Each curve describes individual tumour growth (denoted Q, T, GA etc.)

3.2.2. Tumour growth-rate is negatively associated with the frequency and amplitudes of the VD oscillations

For studying the relationships between the tumour growth-rates and vascular dynamics, we clustered the empirical results into three arbitrarily defined groups, according to the apparent tumour growth-rate: (i) relatively fast tumour growth-rate – reaching approximately 30–60 mm^3 in 1 month (tumours "K", "Y", "U", Fig. 4(a)); (ii) moderate tumour growth-rate – reaching approximately 10–30 mm^3 in 1 month (tumours "Q", "T", "GA", Fig. 4(b)); (iii) relatively slow tumour growth-rate – reaching 1–10 mm^3 in 1 month (tumours "A", "I", "S", Fig. 4(c)). For consistency, we have excluded from this analysis the tumours whose average VD measurements were calibrated in relation to a different control region (see Section 2).

Individual tumour growth-rates, calculated over short time intervals, were plotted as a function of AVD. Results suggest that the increase in overall tumour volume was negatively related to the variability in the AVD measurements, and to the variability in the tumour growth-rates. Note that the most vigorously growing tumours had no fluctuations in the tumour growth-rate, while their AVD varied within a small range of values (0.665–1.3 units of signal intensity; Fig. 4(a)). In the slow-growing tumours (Fig. 4(c)), the fluctuations in tumour growth-rates and in AVD are more significant than those of the moderately growing tumours (Fig. 4(b)).

The empirical AVD of individual tumours (Fig. 5(a)–(c)), were compared with the model predictions

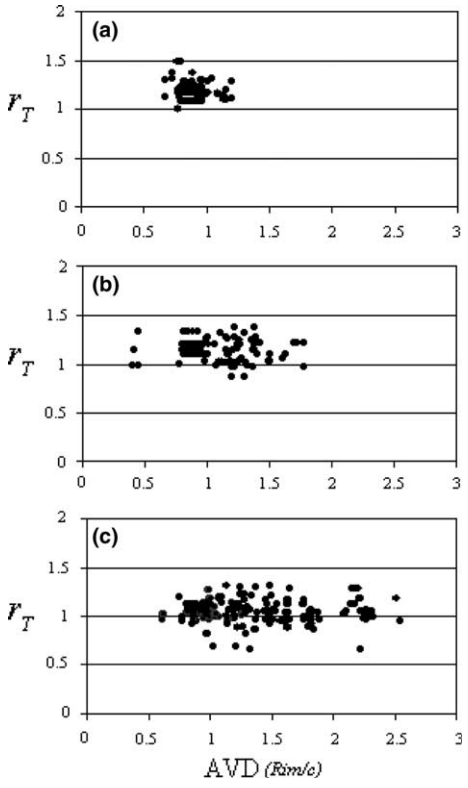

Fig. 4. Experimental *in vivo* results showing tumour growth-rates as a function of AVD (for dimensions see note in Fig. 2) . Individual tumour growth-rate calculated for short time intervals, r_T, were mapped on the respective AVD measurements which were normalised by the control areas, c, for groups of fast-(a), moderate-(b) and slow-(c) growing tumours. Group "A" included the tumours: "K", "Y", "U"; Group "B" included the tumours: "Q", "T", "GA"; Group "C" included the tumours: "A", "I", "S". In this figure, AVD values were normalised by the control tissue "c", rather than "d", as it was closer to the tumour and had more reliable input dataset, due to the limitations of the technique.

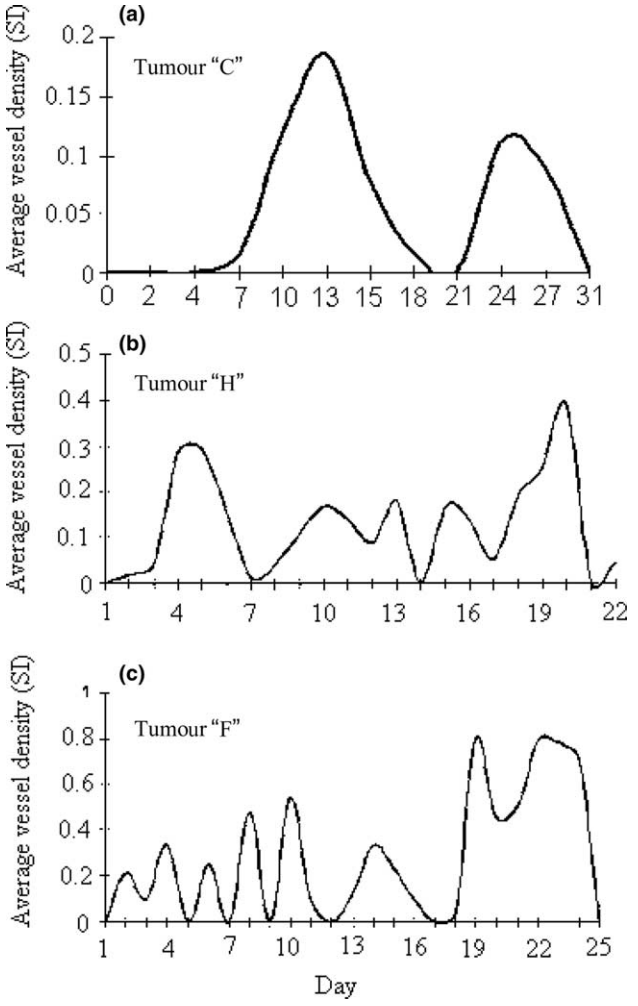

Fig. 5. Measurements of AVD as a function of time (in days), in three individual tumours, as detected noninvasively by MRI (For dimensions, see note in Fig. 2). Each extreme point represents one measurement and the intermediate points were extrapolated by observed changes in tumour volume. Two maxima in AVD are observed in the fast-growing tumour (a); a pattern of two high peaks, intermittent with two or three smaller VD peaks is observed for the moderately growing tumour (b); AVD pattern of frequent fluctuations, whose amplitudes increase over time is observed for the slow-growing tumour (c).

(Fig. 2(a)–(c)). Comparison shows that the predicted and observed apparent VD had similar dynamic profiles, in spite of their different "resolutions" (the empirical VD was read in 2–3 day intervals, whereas simulation results were recorded every 6 h). Thus, a similar, double maximum pattern is both predicted and observed empirically for fast-growing tumours (Fig. 2(a)(II) compared with Fig. 5(a)), and a pattern of frequently fluctuating VD, with larger amplitude than in faster growing tumours, is both predicted and empirically observed in slow-growing tumours (Fig. 2(c)(II) compared with Fig. 5(c)). In general, the observation of increasing frequency of AVD oscillations, coinciding with decreasing tumour growth capacity is in accordance with the model's predictions.

3.2.3. Microenvironmental dependence of MatVD and ImmVD

We analysed the dynamics of new vessel formation and of vessel maturation in individual tumours. Such analysis was mandatory for verifying the mathematical model's assumptions that neo-vascularisation and immature vessel maturation, as well as immature and mature vessel regression, can significantly affect tumour growth. Subsequently, this analysis was used for studying the dependence of each of these dynamical processes on other measurable factors in the system.

For analysing the processes of new blood vessel formation and regression separately from those of maturation and mature vessel destabilisation, we used the calibrated measurements of maturation and function. Maturation dynamics are manifested in an increase or decrease in MatVD, relative to the changes in tumour volume. In addition, by subtracting the density of ma-

ture vessels from that of the total functional vessels, measured at the same moment, we estimated the density of newly formed blood vessels and, subsequently, identified regression of the newly formed vessels, at any time during tumour progression.

Measurements of FunVD and MatVD inside the tumour, FunVD(in), MatVD(in), respectively, and at the tumour's rim were normalised by similar measurements in the normal close tissue (c) or at a distance from the tumour site (d). Shown in Fig. 6 are the empirical calibrated MRI readings of VD(in) dynamics in tumours with varying growth-rates. The calibrated MRI readings of MatVD demonstrates the validity of our model's assumption that vessel maturation and destabilisation of mature vessels are dynamic processes occurring concurrently with tumour neovascularisation, both at the core of the tumour and at its rim (as shown in [21]); maturation or destabilisation are manifested in increased or decreased (MatVD) measurements, for a constant tumour volume during a certain period of time (Fig. 6(d), (f)). Moreover, a relative increase or decrease in FunVD, unaccompanied by an increase or decrease in MatVD was interpreted as formation and obliteration of immature vessels, respectively.

The experimental measurements, shown in Fig. 6, support the model prediction in showing that, at any moment of the experiment, the proportion of immature vessels is small in exponentially growing tumours (compare with Fig. 2(a) and (b)). Note that the apparently decreasing density of mature vessels in these figures, which is also observed in the simulations (Fig. 2(a)(I)), probably reflects dilution, as these tumours undergo rapid volume increase during the first month of growth. In somewhat less vigorous tumours, FunVD is shown to increase in the first weeks of tumour growth. However, here too, newly formed vessels seem to mature relatively quickly, so that immature vessels are hardly detected (Fig. 6(c)). In more moderately growing tumours, the

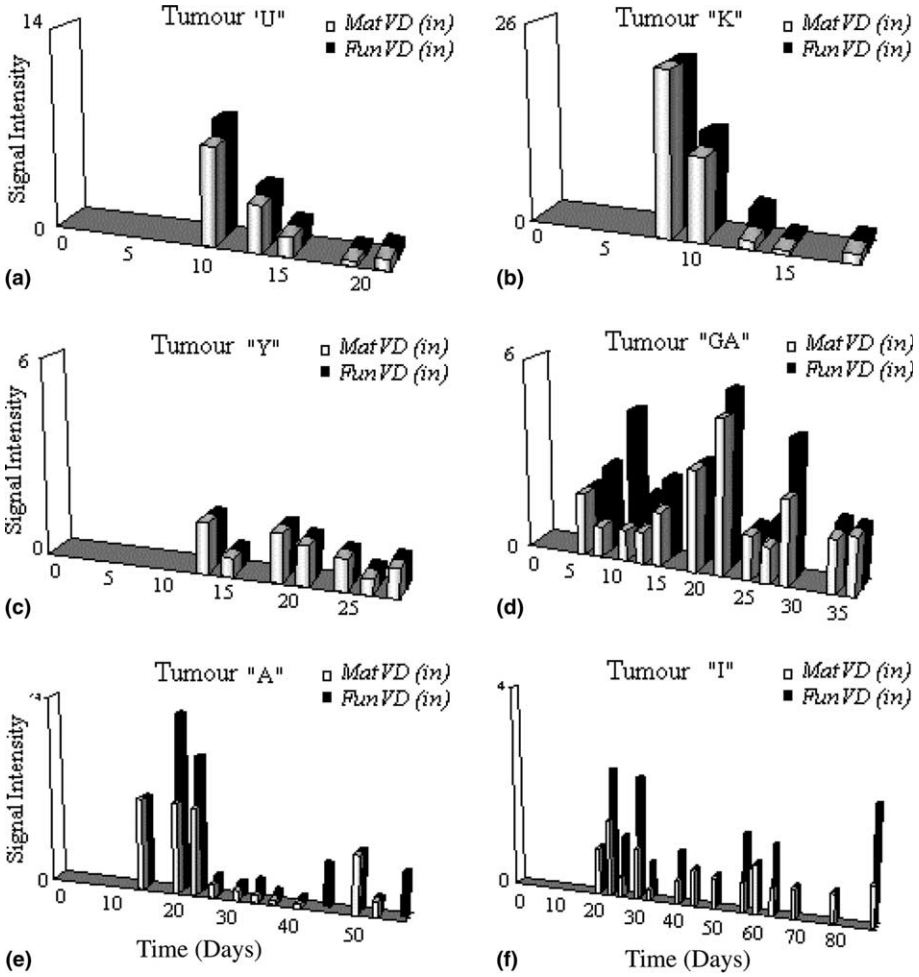

Fig. 6. Dynamics of FunVD and MatVD measured *in vivo* at the tumour core (FunVD(in), MatVD(in), respectively). The difference between MatVD(in) and FunVD(in) at a given time-point indicates the density of new blood vessels, ImmVD. The measurements were normalised by similar measurements in the normal host tissue close to the tumour site (c) ; tumours "Y" and "U" were normalised by the far control point, d. One should note that this figure portrays calibrated measurements of mature and functional vessel density and not AVD (see Section 2). (a)–(f) represent different tumour.

newly formed vessels constitute a larger proportion of the overall functional vessels. Here, the period of oscillation in ImmVD is smaller than that in maturation-destabilisation, indicating a somewhat slower maturation-rate, presumably due to a poor microenvironment. Consequently, the two processes are desynchronised in these tumours and, as our model suggested, a maximum in FunVD can coincide with a minimum in MatVD (Fig. 5(d) and (e)). The angiogenesis rate exceeds the maturation-rate in the slowest growing tumours. Therefore, significant angiogenesis and, consequently, regression of the unprotected newly formed vessels can be detected (Fig. 6(f)). It should be re-emphasised that this result does not necessarily imply that in slow-growing tumours angiogenesis is more active than in faster growing tumours, but, rather, that in slow-tumours maturation is less efficient.

4. Discussion

Based on the computer simulations of the model, we assert that the heterogeneity in the tumour growth-rate is sufficiently accounted for by the variation in microenvironmental density of blood vessels. Thus, in microenvironments having large MatVD, the rate of vessel maturation is expected to balance the rate of neo-vascularisation. The outcome should be monotonic processes of vascular and tumour growth, and, as a consequence, a higher average tumour growth-rate. In contrast, low MatVD in the microenvironment is expected to slowdown the maturation of newly formed vessels, so that the proportion of immature vessels will be relatively large and the two processes will be only loosely balanced. These fragile immature vessels regress in size, perfusion decreases and, as a result, a new cycle of angiogenesis is started. This oscillating pattern is expected to cause decreasing overall tumour growth capacity, suggesting that ovary carcinoma metastases of a common origin can vary significantly in their growth-rates, depending on the VD in their seeding sites.

In general, our analysis of the empirical results confirms the above mathematical model's predictions. The experiments reported here suggest that during the first few weeks following implantation of human ovary carcinoma spheroids in mice, a lower tumour growth capacity was associated with lower proportions of mature vessels in the tumour, and with a looser synchronisation of neovasculature formation and maturation. Our analysis of the experimental results further confirms the model's assumptions of interactive processes of angiogenesis, regression, maturation and destabilisation. Together, these processes form an oscillatory pattern of VD in the growing tumour, whose period varies in association with the tumour growth capacity. It may be worthwhile to check the validity of this conclusion in different experimental scenarios, different cell lines and different cancer types.

Our results support the findings of Monsky and colleagues [25] who studied vasculature properties in primary and metastatic breast tumours and suggested that vascular permeability in tumours implanted in the mammary fat pad is higher than in those implanted in cranial windows. The authors conclude that the host microenvironment plays a significant role in determining gene expression and physiological functions of tumour vasculatures and propose that higher VD and blood flow in the underlying pial tissue may potentiate the angiogenic response to tumour factors. In accordance, our simulations showed that a large variation in VD at the tumour implantation site explains the variation in the tumour growth-rate. Our analysis of the *in vivo* tumour implantation experiments shows that accelerated tumour growth is associated with a relatively small fraction of immature vessels, which, inevitably, is associated with a low permeability. Interestingly, Monsky and colleagues caution that a higher expression of angiogenic growth factors is not a good surrogate marker of VD. Indeed, our simulations suggest significant oscillations in angiogenesis related growth factors (see [6,26]). These simulations can explain why growth-factor concentrations evaluated at the peak of the oscillations can not be a good marker of their average tumour-specific concentration. In our work, the highly variable empirical growth patterns were retrieved by the same underlying dynamic model where immature and mature vessels have different reaction rates and individual tumours were implanted in varying vascular beds.

In this work, we validated the mathematical model's capacity to retrieve *in vivo* vessel dynamics, and to further illuminate associated biological phenomena that are intractable to experimental analysis. Further retrospective validation of our model has been done using results of untreated [27] and treated [28] human breast cancer and human brain carcinoma [29] (data not shown). After verifying its accuracy in prospective human clinical trials, the computerised mathematical model will be employed for predicting the comprehensive feedback effects on VD, including those of specific cytotoxic and cytostatic therapy, at every moment of tumour progression, in primary and metastatic disease.

Conflict of interest

None declared.

Acknowledgements

The analytical work was supported by research grants from the European Union (HPRN-CT-2000-

00105) and the Chai Foundation. LA was partly supported by the Israeli Ministry of Absorption. The empirical mice experiments were carried out under the support of the Israeli Ministry of Health (Research Grant IMOH6944 to Michal Neeman and Zvia Agur). We thank Michal Neeman and Assaf Gilead for carrying out the mice experiments analysed in this work, Vladimir Vainstein for useful discussion and Yechiel Goldman for critically reading the manuscript.

References

1. Carmeliet P, Jain RK. Angiogenesis in cancer and other diseases. *Nature* 2000, **407**, 249–257.
2. Yancopoulos GD, Davis S, Gale NW, Rudge JS, Wiegand SJ, Holash J. Vascular-specific growth factors and blood vessel formation. *Nature* 2000, **407**, 242–248.
3. Kerbel RS. Tumour angiogenesis: past, present and the near future. *Carcinogenesis* 2000, **21**, 505–515.
4. Danielsen T, Rofstad EK. The constitutive level of vascular endothelial growth factor (VEGF) is more important than hypoxia-induced VEGF up-regulation in the angiogenesis of human melanoma xenografts. *Br J Cancer* 2000, **82**, 1528–1534.
5. Dor Y, Porat R, Keshet E. Vascular endothelial growth factor and vascular adjustments to perturbations in oxygen homeostasis. *Am J Physiol Cell Physiol* 2000, **280**, C1367–C1374.
6. Arakelyan L, Vainstein V, Agur Z. A computer algorithm describing angiogenesis and vessel maturation and its use for studying the effects of anti-angiogenic and anti-maturation therapy on vascular tumour growth. *Angiogenesis* 2002, **5**, 203–214.
7. Agur Z, Arakelyan L, Daugulis P, Ginosar Y. Hopf point analysis for angiogenesis models. *Discret Contin Dyn S – Series B* 2004, **4**, 29–38.
8. Eberhard A, Kahlert S, Goede V, Hemmerlein B, Plate KH, Augustin HG. Heterogenity of angiogenesis and blood vessel maturation in human tumors: implications for antiangiogenic tumour therapies. *Cancer Res* 2000, **60**, 1388–1393.
9. Gee MS, Procopio WN, Makonnen S, Feldman MD, Yeilding WM, Lee WM. Tumor vessel development and maturation impose limits on the effectiveness of anti-vascular therapy. *Am J Pathol* 2003, **162**, 183–193.
10. Breier G, Albrecht U, Sterrer S, Risau W. Expression of vascular endothelial growth factor during embryonic angiogenesis and endothelial cell differentiation. *Development* 1992, **114**, 521–532.
11. Benjamin LE, Hemo I, Keshet E. A plasticity window for blood vessel remodelling is defined by pericyte coverage of the preformed endothelial network and is regulated by PDGF-B and VEGF. *Development* 1998, **125**, 1591–1598.
12. Ferrara N, Henzel WJ. Pituitary follicular cells secrete a novel-heparin – binding growth factor specific for vascular endothelial cells. *Biochem Biophys Res Commun* 1989, **161**, 851–858.
13. Shweiki D, Itin A, Soffer D, Keshet E. Vascular endothelial growth factor induced by hypoxia may mediate hypoxia-initiated angiogenesis. *Nature* 1992, **359**, 843–845.
14. Ferrara N, Houck K, Jakeman L, Leung DW. Molecular and biological properties of the vascular endothelial growth factor family of proteins. *Endocr Rev* 1992, **13**, 18–32.
15. Ferrara N, Carver-Moore K, Chen H, *et al*. Heterozygous embryonic lethality induced by targeted inactivation of the VEGF gene. *Nature* 1996, **380**, 439–442.
16. Carmeliet P, Ferreira V, Breier G, *et al*. Abnormal blood vessel development and lethality in embryos lacking a single VEGF allele. *Nature* 1996, **380**, 435–439.
17. Manegold PC, Hutter J, Pahernik SA, Messmer K, Dellian M. Platelet–endothelial interaction in tumor angiogenesis and microcirculation. *Blood* 2003, **101**, 1970–1976.
18. Hirschi KK, Rohovsky SA, Beck LH, Smith SR, D'Amore PA. Endothelial cells modulate the proliferation of mural cell precursors via PDGF-BB and heterotypic cell contact. *Circ Res* 1999, **84**, 298–305.
19. Maisonpierre PC, Suri C, Jones PF, Bartunkova S, Wiegand SJ, Radziejewski C, *et al*. Angiopoietin-2, a natural antagonist for tie2 that distrupts in vivo angiogenesis. *Science* 1997, **277**, 55–60.
20. Gilead A, Neeman M. Dynamic remodeling of the vascular bed precedes tumor growth: MLS ovarian carcinoma spheroids implanted in nude mice. *Neoplasia* 1999, **1**, 226–230.
21. Gilead A, Meir G, Neeman M. The role of angiogenesis, vascular maturation, regression and stroma infiltration in dormancy and growth of implanted MLS ovarian carcinoma spheroids. *Int J Cancer* 2004, **108**, 524–531.
22. Abramovitch R, Dafni H, Smouha E, *et al*. In vivo prediction of vascular susceptibility to vascular endothelial growth factor withdrawal: magnetic resonance imaging of C6 rat glioma in nude mice. *Cancer Res* 1999, **59**, 5012–5016.
23. Abramovitch R, Frenkiel D, Neeman M. Analysis of subcutaneous angiogenesis by gradient echo magnetic resonance imaging. *Magn Reson Med* 1998, **39**, 813–824.
24. Hart D, Shochat E, Agur Z. The growth law of primary breast cancer tumors as inferred from mammography screening trials. *Br J Cancer* 1998, **78**, 382–387.
25. Monsky WL, Mouta CC, Tsuzuki Y, Gohongi T, Fukumura D, Jain RK. Role of host microenvironment in angiogenesis and microvascular functions in human breast cancer xenografts: mammary fat pad versus cranial tumors. *Clin Cancer Res* 2002, **8**, 1008–1013.
26. Arakelyan L, Vainstein V, Agur Z. Optimizing anti-angiogenic therapy using mathematical tools In: Proceedings of American Society of Clinical Oncology (ASCO), vol. 21, 2002, 440a.
27. Heuser L, Spratt JS, Polk HC. Growth-rates of primary breast cancers. *Cancer* 1979, **43**, 1888–1894.
28. Chang JC, Wooten EC, Tsimelzon A, Hilsenbeck SG, Gutierrez R, Elledge R, *et al*. Gene expression profiling for the prediction of therapeutic response to docetaxel in patients with breast cancer. *Lancet* 2003, **362**, 362–369.
29. Mandonnet E, Delattre JY, Tanguy ML, Swanson KR, Carpentier AF, Duffau H, *et al*. Continuous growth of mean tumor diameter in a subset of grade II gliomas. *Ann Neurol* 2003, **53**, 524–528.